

Non-Synchronous Motions Near Critical Speeds in a Single-Plane Auto-Balancing Device

B. Ryzhik, L. Sperling, H. Duckstein

Automatic balancing devices comprising several balls or other moving elements in circular tracks can efficiently compensate rigid rotor unbalance in certain ranges of rotational speed. However, near critical speeds the vibration level can be comparatively high as a result of non-synchronous ball motions. The paper considers such non-synchronous motions of balancing elements. The characteristics of ball motions and the main factors influencing the investigated phenomenon are analyzed. The paper includes an analytical study of non-synchronous motions, results of computer simulations and comparison with experimental data. Recommendations are given for the optimal choice of auto-balancing device parameters and other measures for decreasing vibrations near critical speeds.

1 Introduction

Rigid rotor auto-balancing devices comprising balls or rollers in circular tracks for compensating unbalanced inertia forces are the subject of investigation for many researchers. Thearle (1932) was the first to introduce such device with one track and two balls. Later, the device was generalized by Hedaya and Sharp, who proposed a two-plane device with four balls for compensating both unbalanced force and unbalanced moment of rigid rotor (Hedaya and Sharp, 1977). The interest in auto-balancing and the number of publications on this subject have been noticeably increasing in recent times (Bövik and Högfors, 1986; Chung and Ro, 1999; Kang et al., 2001; Huang and Chao, 2002; Olsson, 2002). Some principal aspects of automatic balancing were investigated in publications by Sperling et al. (Sperling and Duckstein, 2001a; Sperling et al., 2002; Sperling et al., 2001b; Ryzhik et al., 2002a). Auto-balancing is particularly advantageous for rotors with variable unbalance, such as washing machines, centrifuges, grinding machines, and CD-ROM drives.

The main attention of researchers is focused on the possibility and stability of unbalance compensation by means of auto-balancing devices. Therefore, investigations usually concentrate on synchronous motions, where the balls and the rotor have equal speeds. Meanwhile, experimental data confirmed by simulation results revealed that a different type of motion may occur in the regions near the critical speeds of the rotor system. Under specific conditions during rotor run-up, the balls exhibit non-synchronous motions, continuing to move with speeds close to the rotor eigenfrequency, whereas the rotor gains in speed and passes the critical speed area. This phenomenon is similar (but not completely identical) to the well-known Sommerfeld-effect in unbalanced rotor systems with a limited driving moment.

The non-synchronous motion of the balls is an undesirable phenomenon in automatic balancing as it may cause high vibrations near critical speeds. If parameters are not properly chosen, such vibrations may significantly exceed the magnitude of vibrations of a rotor system without auto-balancing device.

The display of non-synchronous motions in automatic balancing was first revealed in (Sperling et al., 2002; Sperling et al., 2001b; Ryzhik et al., 2002a; Duckstein et al., 1999). The systematic analysis of the important particular case, when the rotor with a single-plane auto-balancing device is symmetrically supported and has only static unbalance, was performed in Ryzhik et al. (Ryzhik et al., 2001; Ryzhik et al., 2002b). In the present publication we consider a general case of a statically and dynamically unbalanced rigid rotor with a single-plane auto-balancing device, presenting analytical study, detailed simulation results and experimental data.

2 Model and Equations of Motion

Figure 1 demonstrates a rigid rotor with auto-balancing device. The axial-symmetric rotor has a mass m_R and moments of inertia $J_{xxR} = J_{yyR} = J_{aR}$, $J_{zzR} = J_{zR}$, $J_{xyR} = J_{yzR} = J_{zxR} = 0$ with respect to the center of mass in the non-rotating vector frame $\vec{e}_x, \vec{e}_y, \vec{e}_z$; $q_V = [r_x \ \psi_y \ r_y \ \psi_x]^T$ are the co-ordinates of the vibrational motion (see Figure 2). The rotor has m unbalances in the planes z_k ($k = n+1, \dots, n+m$), hereinafter referred to as primary

unbalances, idealized as mass points with masses m_k and eccentricities ε_k . The rotor angular velocity is $\dot{\varphi}_R$; the angular positions of primary unbalances are $\varphi_k = \varphi_R + \alpha_k$, $k = n+1, \dots, n+m$.

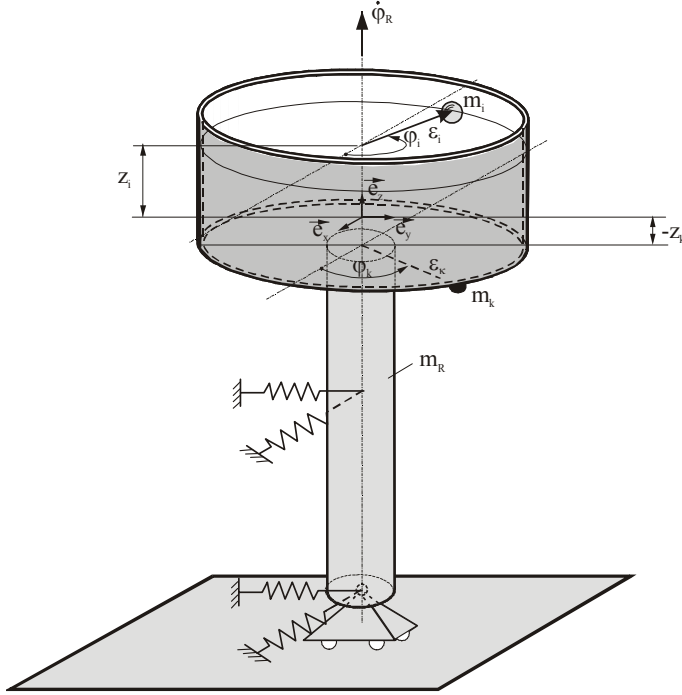


Figure 1. Rotor model

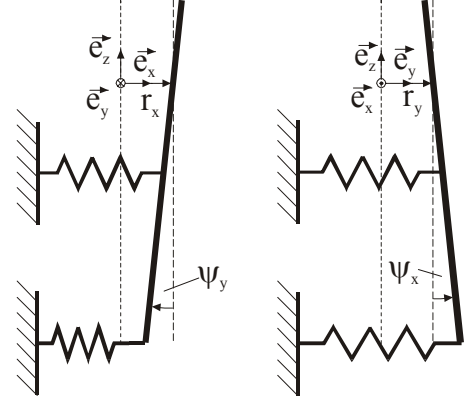


Figure 2. Main system variables

The angular co-ordinate φ_i , $i = 1, \dots, n$, describes the motion of a compensation element of the auto-balancing device (see Figure 1), characterized by the mass, the eccentricity of the mass center, the radius, the position of plane (m_i , ε_i , r_i , z_i , $i = 1, \dots, n$ respectively), and the moments of inertia $J_{xxi} = J_{yyi} = J_{q_i}$, $J_{zzi} = J_{p_i}$, $J_{xyi} = J_{yzi} = J_{zxi} = 0$ with respect to the center of mass. It is assumed that the elements roll along the tracks without slipping and viscous medium exerts damping moment on them. Considering also external damping, the overall damping moment acting upon the rotor is (Sperling et al., 2002)

$$M_d = - \left[\bar{\beta}_R \dot{\varphi}_R + \sum_{i=1}^n \beta_i (\dot{\varphi}_R - \dot{\varphi}_i) \right] = -\beta_R \dot{\varphi}_R + \sum_{i=1}^n \beta_i \dot{\varphi}_i, \quad \beta_R = \bar{\beta}_R + \sum_{i=1}^n \beta_i. \quad (1)$$

The isotropic elastic damping supports are characterized by the stiffness parameters k_{11} , k_{12} , k_{22} and the damping parameters c_{11} , c_{12} , c_{22} with respect to the vibrational co-ordinates \mathbf{q}_V ; $L_R = L_R(\dot{\varphi}_R)$ is the rotor driving torque.

Using the abbreviations

$$\begin{aligned} M &= m_R + \sum_{i=1}^{n+m} m_i, & J_{bi} &= \frac{2}{5} m_i r_i^2, & i &= 1, \dots, n, \\ J_a &= J_{aR} + \sum_{i=1}^{n+m} m_i z_i^2 + \sum_{i=1}^n J_{bi}, & J_z &= J_{zR} + \sum_{i=1}^n \left(\frac{R_i}{r_i} \right)^2 J_{bi} + \sum_{i=n+1}^{n+m} m_i \varepsilon_i^2, \\ \tilde{J}_z &= J_{zR} + \sum_{i=1}^n \frac{R_i}{r_i} J_{bi}, & \tilde{J}_i &= \begin{cases} m_i \varepsilon_i \left(\varepsilon_i - \frac{2}{5} r_i \right), & i = 1, \dots, n, \\ m_i \varepsilon_i^2, & i = m+1, \dots, n+m, \end{cases} \\ J_i &= \frac{7}{5} m_i \varepsilon_i^2, & J_{iR} &= \frac{R_i \varepsilon_i}{r_i^2} J_{bi}, & i &= 1, \dots, n, \end{aligned} \quad (2)$$

we obtain the following Lagrange's equations for the system under investigation, linearized in the vibrational co-ordinates \mathbf{q}_V (Sperling et al., 2002; Sperling et al., 2001b)

$$M\ddot{r}_x + \sum_{k=1}^{n+m} m_k z_k \ddot{\psi}_y + c_{11}\dot{r}_x + c_{12}\dot{\psi}_y + k_{11}r_x + k_{12}\psi_y = \sum_{k=1}^{n+m} m_k \varepsilon_k (\ddot{\phi}_k \sin \varphi_k + \dot{\phi}_k^2 \cos \varphi_k), \quad (3)$$

$$\begin{aligned} & \sum_{k=1}^{n+m} m_k z_k \ddot{r}_x + J_a \ddot{\psi}_y + \frac{1}{2} \sum_{k=1}^{n+m} m_k \varepsilon_k^2 [-\ddot{\psi}_x \sin 2\varphi_k + \ddot{\psi}_y (1 + \cos 2\varphi_k)] \\ & + c_{12}\dot{r}_x + c_{22}\dot{\psi}_y - \left[\tilde{J}_z \dot{\phi}_R + \sum_{k=1}^{n+m} \tilde{J}_k \dot{\phi}_k \right] \dot{\psi}_x - \sum_{k=1}^{n+m} m_k \varepsilon_k^2 \dot{\phi}_k (\dot{\psi}_x \cos 2\varphi_k + \dot{\psi}_y \sin 2\varphi_k) \\ & + k_{12}\dot{r}_x + k_{22}\dot{\psi}_y - \frac{1}{2} \left[\tilde{J}_z \ddot{\phi}_R + \sum_{k=1}^{n+m} \tilde{J}_k \ddot{\phi}_k \right] \psi_x = \sum_{k=1}^{n+m} m_k \varepsilon_k z_k (\ddot{\phi}_k \sin \varphi_k + \dot{\phi}_k^2 \cos \varphi_k), \end{aligned} \quad (4)$$

$$M\ddot{r}_y - \sum_{k=1}^{n+m} m_k z_k \ddot{\psi}_x + c_{11}\dot{r}_y - c_{12}\dot{\psi}_x + k_{11}r_y - k_{12}\psi_x = - \sum_{k=1}^{n+m} m_k \varepsilon_k (\ddot{\phi}_k \cos \varphi_k - \dot{\phi}_k^2 \sin \varphi_k) \quad (5)$$

$$\begin{aligned} & - \sum_{k=1}^{n+m} m_k z_k \ddot{r}_y + J_a \ddot{\psi}_x + \frac{1}{2} \sum_{k=1}^{n+m} m_k \varepsilon_k^2 [\ddot{\psi}_x (1 - \cos 2\varphi_k) - \ddot{\psi}_y \sin 2\varphi_k] \\ & - c_{12}\dot{r}_y + c_{22}\dot{\psi}_x + \left[\tilde{J}_z \dot{\phi}_R + \sum_{k=1}^{n+m} \tilde{J}_k \dot{\phi}_k \right] \dot{\psi}_y + \sum_{k=1}^{n+m} m_k \varepsilon_k^2 \dot{\phi}_k (\dot{\psi}_x \sin 2\varphi_k - \dot{\psi}_y \cos 2\varphi_k) \\ & - k_{12}\dot{r}_y + k_{22}\dot{\psi}_x + \frac{1}{2} \left[\tilde{J}_z \ddot{\phi}_R + \sum_{k=1}^{n+m} \tilde{J}_k \ddot{\phi}_k \right] \psi_y = \sum_{k=1}^{n+m} m_k \varepsilon_k z_k (\ddot{\phi}_k \cos \varphi_k - \dot{\phi}_k^2 \sin \varphi_k), \end{aligned} \quad (6)$$

$$J_z \ddot{\phi}_R - \sum_{k=1}^n J_{kR} \ddot{\phi}_k + \beta_R \dot{\phi}_R - \sum_{k=1}^n \beta_k \dot{\phi}_k - \sum_{k=n+1}^{n+m} m_k \varepsilon_k [\dot{r}_{kx} \sin \varphi_k - \dot{r}_{ky} \cos \varphi_k] = L_R(\dot{\phi}_R), \quad (7)$$

$$-J_{kR} \ddot{\phi}_R + J_k \ddot{\phi}_i - \beta_k \dot{\phi}_R + \beta_k \dot{\phi}_k - m_k \varepsilon_k [\dot{r}_{kx} \sin \varphi_k - \dot{r}_{ky} \cos \varphi_k] = 0, \quad k = 1, \dots, n \quad (8)$$

with

$$r_{kx} = r_x + z_k \psi_y, \quad r_{ky} = r_y - z_k \psi_x, \quad k = 1, \dots, n+m. \quad (9)$$

The equations (3)-(8) represent a general system of equations of motion for the rotor with several primary unbalances and several tracks with auto-balancing balls. To simplify description of the considered effect, we investigate below the simpler case in which the rotor has only one primary unbalance and a single auto-balancing track with n elements. We assume that the primary unbalance plane does not coincide with the plane of the auto-balancing device and neither are placed in the plane of rotor center of mass, so the rotor is statically and dynamically unbalanced.

3 Analytical Study

In the analytical investigation we consider a quasi-stationary process: we assume that driving moment L_R and rotor speed ω_R change slowly, at every moment they can be considered as constant. For convenience, we characterize the driving moment by the ‘‘nominal speed’’ $\Omega = \frac{L_R}{\beta_R}$.

Simulations confirmed by experimental data reveal that near critical speeds balls move ‘‘together’’ in each plane with the same speed, not equal to the rotor speed; moreover, they exhibit the same phase. Using the method of direct separation of motion (Blekhman, 2000), we present the motion of the system for the case when all balls are situated in one plane (single-plane device) in the form

$$\begin{aligned}\varphi_R &= \omega_R t + \zeta_R(qt), & \omega_R &= \text{const.}, & q &= \omega_R - \omega_b, \\ \varphi_k &= \omega_b t + \alpha_k + \zeta_k(qt), & \omega_e &= \text{const.}, & \alpha_k &= \alpha_b = \text{const.}, & k &= 1, \dots, n,\end{aligned}\quad (10)$$

where $\zeta_R(qt), \zeta_k(qt)$ are harmonical functions with frequency q .

Neglecting phase oscillations and small terms on the left hand side, we can rewrite equations (3)-(6) as

$$M\ddot{r}_x + c_{11}\dot{r}_x + c_{12}\dot{\psi}_y + k_{11}r_x + k_{12}\psi_y = m_p \varepsilon_p \omega_R^2 \cos \omega_R t + nm_b \varepsilon_b \omega_b^2 \cos(\omega_b t + \alpha_b), \quad (11)$$

$$\begin{aligned}J_a \ddot{\psi}_y - J_z \dot{\psi}_x \omega_R + c_{12}\dot{r}_x + c_{22}\dot{\psi}_y + k_{12}r_x + k_{22}\psi_y &= \\ &= m_p \varepsilon_p z_p \omega_R^2 \cos \omega_R t + nm_b \varepsilon_b z_b \omega_b^2 \cos(\omega_b t + \alpha_b),\end{aligned}\quad (12)$$

$$M\ddot{r}_y + c_{11}\dot{r}_y - c_{12}\dot{\psi}_x + k_{11}r_y - k_{12}\psi_x = m_p \varepsilon_p \omega_R^2 \sin \omega_R t + nm_b \varepsilon_b \omega_b^2 \sin(\omega_b t + \alpha_b), \quad (13)$$

$$\begin{aligned}J_a \ddot{\psi}_x + J_z \dot{\psi}_y \omega_R - c_{12}\dot{r}_y + c_{22}\dot{\psi}_x - k_{12}r_y + k_{22}\psi_x &= \\ &= -m_p \varepsilon_p z_p \omega_R^2 \sin \omega_R t - nm_b \varepsilon_b z_b \omega_b^2 \sin(\omega_b t + \alpha_b).\end{aligned}\quad (14)$$

The equations (11)-(14) can also be presented in the complex form. Introducing

$$r = r_x + ir_y, \quad \Psi = \psi_y - i\psi_x, \quad (15)$$

we obtain

$$M \ddot{r} + c_{11}\dot{r} + c_{12}\dot{\Psi} + k_{11}r + k_{12}\Psi = m_p \varepsilon_p \omega_R^2 e^{i\omega_R t} + nm_b \varepsilon_b \omega_b^2 e^{i(\omega_b t + \alpha_b)}, \quad (16)$$

$$\begin{aligned}J_a \ddot{\Psi} - J_z i \dot{\Psi} \omega_R + c_{12}\dot{r} + c_{22}\dot{\Psi} + k_{12}r + k_{22}\Psi &= \\ &= m_p \varepsilon_p z_p \omega_R^2 e^{i\omega_R t} + nm_b \varepsilon_b z_b \omega_b^2 e^{i(\omega_b t + \alpha_b)}.\end{aligned}\quad (17)$$

Presenting the solution in the form

$$\begin{aligned}r &= r_p e^{i\omega_R t} + r_b e^{i(\omega_b t + \alpha_b)}, \\ \psi &= \psi_p e^{i\omega_R t} + \psi_b e^{i(\omega_b t + \alpha_b)},\end{aligned}\quad (18)$$

and taking into account that vibrations in the plane with axial co-ordinate z_k are

$$r_k = r + z_k \Psi, \quad (19)$$

we get

$$\begin{aligned}r_k &= (r_p + z_k \psi_p) e^{i\omega_R t} + (r_b + z_k \psi_b) e^{i(\omega_b t + \alpha_b)} = r_{kp} e^{i\omega_R t} + r_{kb} e^{i(\omega_b t + \alpha_b)}, \\ r_{ks} &= m_s \varepsilon_s \omega_s^2 A(\omega_s, \omega_R, z_p, z_p), \quad s = p, b,\end{aligned}\quad (20)$$

where

$$\begin{aligned}A(\omega_s, \omega_R, z_i, z_k) &= N(\omega_s, \omega_R, z_i, z_k) / \Delta(\omega_s, \omega_R), \\ N(\omega_s, \omega_R, z_i, z_k) &= -(J_a \omega_s^2 - J_z \omega_R \omega_s) + \kappa_{22}(\omega_s) - \kappa_{12}(\omega_s) z_k + \\ &\quad + z_i \left[(-M \omega_s^2 + \kappa_{11}(\omega_s)) z_k - \kappa_{12}(\omega_s) \right], \\ \Delta(\omega_s, \omega_R) &= M \omega_s^2 (J_a \omega_s^2 - J_z \omega_R \omega_s) - \left[M \omega^2 \kappa_{22}(\omega_s) + (J_a \omega_s^2 - J_z \omega_R \omega_s) \kappa_{11}(\omega_s) \right] + \\ &\quad + \kappa_{11}(\omega_s) \kappa_{22}(\omega_s) - [\kappa_{12}(\omega_s)]^2\end{aligned}\quad (21)$$

$$\kappa_{ik}(\omega) = k_{ik} + i\omega_s c_{ik}, \quad i, k = 1, 2; \quad s = p, b; \quad \omega_p = \omega_R; \quad i = \sqrt{-1}.$$

Vibrations in the planes of the primary unbalance and auto-balancing device include two components with frequencies ω_R and ω_b

$$\begin{aligned} r_p &= r + z_p \Psi = r_{pp} e^{i\omega_R t} + r_{pb} e^{i(\omega_b t + \alpha_b)}, \\ r_b &= r + z_b \Psi = r_{bp} e^{i\omega_R t} + r_{bb} e^{i(\omega_b t + \alpha_b)}. \end{aligned} \quad (22)$$

Projections of these vibrations on axes x, y are

$$\begin{aligned} r_{px} &= r_{pp} \cos(\omega_R t - \varphi_{pp}) + r_{pb} \cos(\omega_b t + \alpha_b - \varphi_{pb}), \\ r_{py} &= r_{pp} \sin(\omega_R t - \varphi_{pp}) + r_{pb} \sin(\omega_b t + \alpha_b - \varphi_{pb}), \\ r_{bx} &= r_{bp} \cos(\omega_R t - \varphi_{bp}) + r_{bb} \cos(\omega_b t + \alpha_b - \varphi_{bb}), \\ r_{by} &= r_{bp} \sin(\omega_R t - \varphi_{bp}) + r_{bb} \sin(\omega_b t + \alpha_b - \varphi_{bb}), \end{aligned} \quad (23)$$

where $r_{pp}, r_{pb}, r_{bp}, r_{bb}$ are the amplitudes of vibrations in the corresponding planes, caused by the primary unbalances and auto-balancing balls; $\varphi_{pp}, \varphi_{pb}, \varphi_{bp}, \varphi_{bb}$ are the phases of these vibrations

$$\begin{aligned} r_{sp} &= |r_{sp}|, \quad \phi_{sp} = -\arg(r_{sp}), \\ r_{sb} &= |r_{sb}|, \quad \phi_{sb} = -\arg(r_{sb}), \quad s = p, b. \end{aligned} \quad (24)$$

The vibrational terms in equations (7), (8) can be calculated as

$$\begin{aligned} B_p &= -m_p \varepsilon_p (\ddot{r}_{px} \sin \omega_R t - \ddot{r}_{py} \cos \omega_R t) = m_p \varepsilon_p \operatorname{Im}(\ddot{r}_p e^{-i\omega_R t}) \\ &= -m_p \varepsilon_p \left[\omega_R^2 \operatorname{Im}(r_{pp}) + \omega_b^2 \operatorname{Im}(r_{pb} e^{-i(\omega_b t + \alpha_b)}) \right], \\ B_i &= -m_b \varepsilon_b \left[\ddot{r}_{bx} \sin(\omega_b t + \alpha_b) - \ddot{r}_{by} \cos(\omega_b t + \alpha_b) \right] = m_b \varepsilon_b \operatorname{Im}(\ddot{r}_b e^{-i(\omega_b t + \alpha_b)}) \\ &= -m_b \varepsilon_b \left[\omega_R^2 \operatorname{Im}(r_{bp} e^{i(\omega_R t - \varphi_{bp})}) + \omega_b^2 \operatorname{Im}(r_{bb}) \right]. \end{aligned} \quad (25)$$

Following the method of direct separation of motion, we replace these terms by the averaged ‘‘vibrational moments’’

$$\begin{aligned} V_p &= \int_0^{2\pi} B_p d(qt) = -m_p \varepsilon_p \omega_R^2 \operatorname{Im}(r_{pp}), \\ V_i &= \int_0^{2\pi} B_i d(qt) = -m_b \varepsilon_b \omega_b^2 \operatorname{Im}(r_{bb}). \end{aligned} \quad (26)$$

The substitution in equations (7), (8) gives

$$\begin{aligned} \beta_R \omega_R - n \beta_b \omega_b - m_p \varepsilon_p \omega_R^2 \operatorname{Im}(r_{pp}) &= \beta_R \Omega, \\ \beta_b \omega_b - m_b \varepsilon_b \omega_b^2 \operatorname{Im}(r_{bb}) &= \beta_b \omega_R. \end{aligned} \quad (27)$$

Using (20)-(24) we can rewrite equations (27) as

$$\beta_R \omega_R - n \beta_b \omega_b - m_p^2 \varepsilon_p^2 \omega_R^4 \operatorname{Im} \left(A(\omega_R, \omega_R, z_p, z_p) \right) = \beta_R \Omega, \quad (28)$$

$$\beta_b \omega_b - n m_b^2 \varepsilon_b^2 \omega_b^4 \operatorname{Im} \left(A(\omega_b, \omega_R, z_b, z_b) \right) = \beta_b \omega_R. \quad (29)$$

Relations (28)-(29) with (21) represent a system of equations for determination of the parameters of non-synchronous motions.

Equations (28)-(29) contain only variables of the ‘‘real’’ type. From (21)

$$\operatorname{Im} \left(A(\omega_s, \omega_R, z_i, z_k) \right) = \frac{\operatorname{Im}(N(\omega_s, z_i, z_k)) \operatorname{Re}(\Delta(\omega_s, \omega_R)) - \operatorname{Im}(\Delta(\omega_s, \omega_R)) \operatorname{Re}(N(\omega_s, \omega_R, z_i, z_k))}{[\operatorname{Re}(\Delta(\omega_s, \omega_R))]^2 + [\operatorname{Im}(\Delta(\omega_s, \omega_R))]^2},$$

$$\begin{aligned}
\operatorname{Re}(\mathbf{N}(\omega_s, \omega_R, z_i, z_k)) &= -(J_a \omega_s^2 - J_z \omega_R \omega_s) + k_{22} - k_{12} z_k + z_i \left[(-M \omega_s^2 + k_{11}) z_k - k_{12} \right], \\
\operatorname{Im}(\mathbf{N}(\omega_s, \omega_R, z_i, z_k)) &= [c_{22} - c_{12} z_k + z_i (c_{11} z_k - c_{12})] \omega_s, \\
\operatorname{Re}(\Delta(\omega_s, \omega_R)) &= M \omega_s^2 (J_a \omega_s^2 - J_z \omega_R \omega_s) - [M \omega_s^2 k_{22} + (J_a \omega_s^2 - J_z \omega_R \omega_s) k_{11}] + \\
&\quad + k_{11} k_{22} - k_{12}^2 - (c_{11} c_{22} - c_{12}^2) \omega_s^2, \\
\operatorname{Im}(\Delta(\omega_s, \omega_R)) &= -[M \omega_s^2 c_{22} + (J_a \omega_s^2 - J_z \omega_R \omega_s) c_{11}] \omega_s + (c_{11} k_{22} + c_{22} k_{11} - 2 c_{12} k_{12}) \omega_s,
\end{aligned} \tag{30}$$

and we obtain a system of equations (28)-(30) of the “real” type.

Below we consider some important particular cases. For the unbalanced rotor without auto-balancing device, only equation (28) without the term $n\beta_b \omega_b$ and equation (30) should be analyzed. From (28) we obtain

$$\beta_R \omega_R - m_p^2 \varepsilon_p^2 \omega_R^4 \operatorname{Im}(\mathbf{A}(\omega_R, \omega_R, z_p, z_p)) = \beta_R \Omega. \tag{31}$$

Equation (31) determines the dependence $\omega_R = \omega_R(\Omega)$. The simplest way to construct this dependence is to build a function

$$\Omega = \Omega(\omega_R) = \omega_R - \frac{1}{\beta_R} m_p^2 \varepsilon_p^2 \omega_R^4 \operatorname{Im}(\mathbf{A}(\omega_R, \omega_R, z_p, z_p)) \tag{32}$$

and inverse it.

The same way we can treat the full system of equations (28)-(29). Equation (29) determines the dependence $\omega_b = \omega_b(\omega_R)$. This equation is more complicated than (31), because the function $\operatorname{Im}(\mathbf{A}(\omega_R, \omega_b, z_b, z_b))$ depends both on the ω_R and ω_b . As above, it is easier to construct the dependence $\omega_R = \omega_R(\omega_b)$, than $\omega_b = \omega_b(\omega_R)$. The inversion of $\omega_R = \omega_R(\omega_b)$ yields $\omega_b = \omega_b(\omega_R)$.

From equation (28)

$$\Omega = \Omega(\omega_b) = \omega_R(\omega_b) - \frac{n\beta_b}{\beta_R} \omega_b - \frac{1}{\beta_R} m_p^2 \varepsilon_p^2 [\omega_R(\omega_b)]^4 \operatorname{Im}(\mathbf{A}(\omega_R(\omega_b), z_p, z_p)). \tag{33}$$

The inversion of (33) gives the dependence $\omega_b = \omega_b(\Omega)$. Combining the dependencies $\omega_R(\omega_b)$ and $\omega_b(\Omega)$ we can construct $\omega_R = \omega_R(\Omega)$.

If damping in the track is low, $n\beta_b \ll \beta_R$, we can neglect the term $n\beta_b \omega_b$ in equation (28). In such cases $\omega_R(\omega_b)$ and $\omega_R(\Omega)$ are independent; the ball motions do not influence the rotor rotation.

4 Numerical and Simulation Results, Estimation of the Border Values

The numerical and simulation results presented below correspond to the rotor system with parameters of the centrifuge rotor. The rotor mass is about 12.5 kg. Its polar moment of inertia is greater than the transverse moment, so the rotor exhibits only one critical speed, approximately 60 rad/s. In simulations, which were performed employing the Advanced Continuous Simulation Language (ACSL), we investigated the transient process of rotor run-up with a slowly increasing driving moment (the nominal speed changes from 0 to $\Omega = \Omega_{\max}$, as in Figure 3).

4.1 Only Primary Unbalance

When the rotor has only primary unbalance, the dependence $\omega_R = \omega_R(\Omega)$ is determined by equation (31). Fig. 4 demonstrates the “analytical” dependence $\omega_R = \omega_R(\Omega)$ and the results of simulation of the transient processes of the rotor run-up.

An analytical study predicts that in the pre-critical region the rotor velocity should be close to the nominal speed. In simulations the picture is slightly different because, due to the acceleration, after the start the rotor speed falls behind the nominal speed. Near the critical speed the analytical and simulation curves merge. In this region one can observe a non-synchronous motion with a noticeable difference between the rotor and the nominal speeds: the rotor speed remains close to the critical speed, while the nominal speed increases. After reaching the border value, the rotor accelerates. In the post-critical area the difference between the rotor and the nominal speeds becomes fairly small.

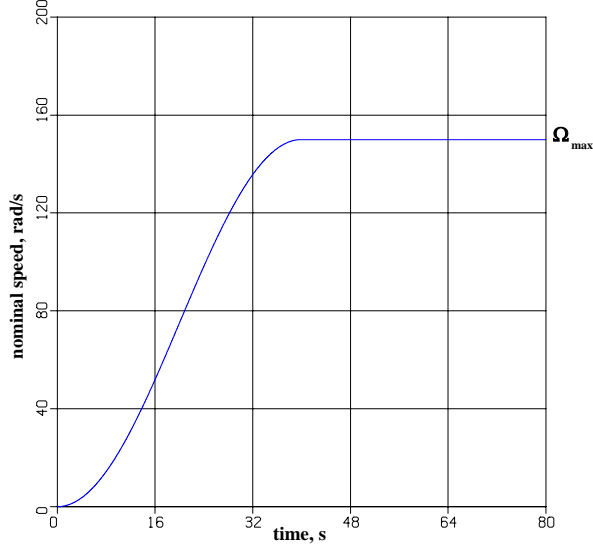


Figure 3. Variation of the nominal speed during the rotor run-up

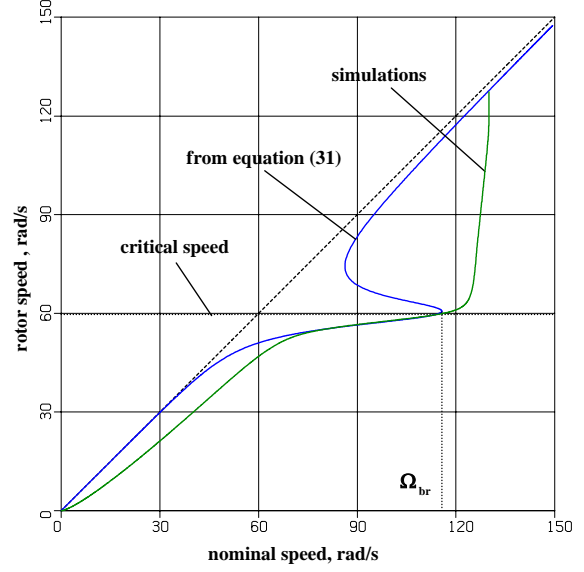


Figure 4. Only primary unbalance. Dependence $\omega_R = \omega_R(\Omega)$

The border value Ω_{br} can be approximately estimated assuming that in the border point $\omega_R(\Omega_{br}) \approx \omega_{cr}$. From (31)

$$\Omega_{br} = \Omega(\omega_{cr}) = \omega_{cr} \left(1 - \frac{1}{\beta_R} m_p^2 \varepsilon_p^2 \omega_{cr}^3 \operatorname{Im} \left(A(\omega_{cr}, \omega_{cr}, z_p, z_p) \right) \right). \quad (34)$$

Calculations show that near the critical speed $\operatorname{Im} \left(A(\omega_{cr}, \omega_{cr}, z_p, z_p) \right) < 0$, so $\Omega_{br} > \omega_{cr}$. Taking into account that $A(\omega_{cr}, \omega_{cr}, z_p, z_p)$ depends only on the properties of rotor and supports and does not depend on parameters of the primary unbalance, we can rewrite (34) in the form

$$\Omega_{br} = \Omega(\omega_{cr}) = \omega_{cr} \left(1 + \frac{1}{\beta_R} m_p^2 \varepsilon_p^2 \omega_{cr}^3 \Phi(M, J_a, J_z, z_p, k_{ik}, c_{ik}) \right). \quad (35)$$

To diminish the area of effect it is necessary to decrease the mass and/or eccentricity of the primary unbalance and to increase the damping parameter β_R .

4.2 Auto-Balancing Device. Dependence $\omega_b = \omega_b(\omega_R)$

In Fig. 5 the dependence $\omega_b = \omega_b(\omega_R)$ numerically calculated from equation (29) is compared with the simulation results. One can see that, for the considered rotor system during the run-up, balls from the start follow the analytical curve. In the critical speed area we can observe noticeable non-synchronous motions. It is interesting that the ball speeds are close to the rotor system eigenvalue, whereas for the classical Sommerfeld-effect in an unbalanced rotor system without auto-balancing device (Fig. 4), the speed of the rotor motion is close to the critical speed of the rotor system.

The border value of non-synchronous motion can be estimated as a point, where the curve $\omega_b = \omega_b(\omega_R)$ crosses the line of eigenvalues, as shown in Fig. 5,6.

The eigenvalue curve $\omega_e = \omega_e(\omega_R)$ corresponds to the condition $\Delta(\omega_e, \omega_R) = 0$ with damping neglected. From (30)

$$M\omega_e^2 (J_a \omega_e^2 - J_z \omega_R \omega_e) - \left[M\omega_e^2 k_{22} + (J_a \omega_e^2 - J_z \omega_R \omega_e) k_{11} \right] + k_{11} k_{22} - k_{12}^2 = 0. \quad (36)$$

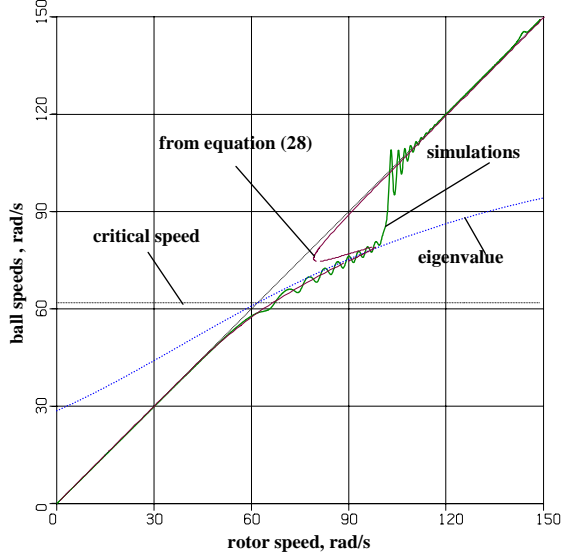


Figure 5. Dependence $\omega_b = \omega_b(\omega_R)$

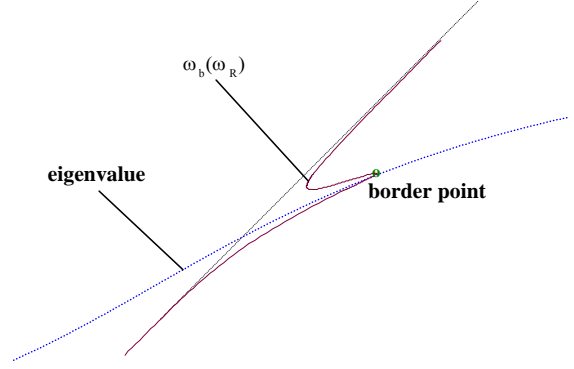


Figure 6. Analytical dependence $\omega_b = \omega_b(\omega_R)$ (fragment near the border point).

As above, we can consider (36) as an equation determining the dependence $\omega_R = \omega_R(\omega_e)$. This yields

$$\omega_R = \frac{MJ_a \omega_e^4 - M \omega_e^2 k_{22} - J_a \omega_e^2 k_{11} + k_{11} k_{22} - k_{12}^2}{MJ_z \omega_e^3 - J_z \omega_e k_{11}}. \quad (37)$$

The dependence $\omega_R = \omega_R(\omega_e)$ has four branches. Selecting the branch, which corresponds to the forward motion in the area of considered critical speed and inverting it, we obtain $\omega_e = \omega_e(\omega_R)$.

To determine the border value of non-synchronous motion we should find $\omega_R = \omega_{Rbr}$ for which $\omega_b(\omega_{Rbr}) = \omega_e(\omega_{Rbr})$. In the border point rotor and ball speeds $\omega_{Rbr}, \omega_{bbr}$ satisfy a system of equations

$$\begin{aligned} \omega_{bbr} - \frac{nm_b^2 \varepsilon_b^2 \omega_{bbr}^4}{\beta_b} \text{Im}(A(\omega_{bbr}, \omega_{Rbr}, z_b, z_b)) &= \omega_{Rbr}, \\ M \omega_{bbr}^2 (J_a \omega_{bbr}^2 - J_z \omega_{Rbr} \omega_{bbr}) - [M \omega_{bbr}^2 k_{22} + (J_a \omega_{bbr}^2 - J_z \omega_{Rbr} \omega_{bbr}) k_{11}] + k_{11} k_{22} - k_{12}^2 &= 0. \end{aligned} \quad (38)$$

The position of border point depends on the rotor system parameters $M, J_a, J_z, z_p, k_{ik}, c_{ik}, i, k = 1, 2$ and on the parameter

$$\sigma = \frac{nm_b^2 \varepsilon_b^2}{\beta_b} \quad (39)$$

characterizing the auto-balancing device and not depending on the primary unbalance. To diminish the area of non-synchronous motion it is necessary to decrease σ , i.e. decrease the mass and/or the eccentricity of the balls and increase the damping parameter β_b .

4.3 Influence of Ball Motions on the Rotor Velocity

For the rotor system serving as the prototype for simulations, damping parameters satisfy the condition $\bar{\beta}_R \gg \beta_b$ and the influence of the ball motions on the rotor velocity is negligible. In general, when damping parameters are of the same order, the influence of ball motions consists in the appearance of the term $n\beta_b \omega_b$ in equation (28). To simplify the construction of dependence $\omega_R = \omega_R(\Omega)$, we can take into account the results of simulations, which revealed that in the region of non-synchronous motions $\omega_b \approx \omega_e(\omega_R)$ and in the post-critical area $\omega_b = \omega_R$.

From (28) we obtain for the first region

$$\beta_R \omega_R - n \beta_b \omega_e(\omega_R) - m_p^2 \varepsilon_p^2 \omega_R^4 \operatorname{Im}(A(\omega_R, \omega_R, z_p, z_p)) = \beta_R \Omega \quad (40)$$

and for the second one

$$(\beta_R - n \beta_b) \omega_R - m_p^2 \varepsilon_p^2 \omega_R^4 \operatorname{Im}(A(\omega_R, \omega_R, z_p, z_p)) = \beta_R \Omega. \quad (41)$$

4.4 Ball Angular Positions

Figs. 7-9 demonstrate ball angular positions during the rotor run-up. In the critical speed area the difference between the rotor and ball speeds is comparatively high due to the non-synchronous motions; the balls lag behind the rotor and move along the track in the direction opposite to rotation. When the area of non-synchronous motions is comparatively wide, the balls accomplish some rounds of the track (Figs. 7,8). When this area is narrow, the balls just make a 180° turn (Fig. 9).

In the critical speed region, balls move together exhibiting the same phase. Analytical investigations predict that in the post-critical range the balls should separate and occupy stable positions which provide zero vibrations in the plane of the device (Ryzhik et al., 2002). But simulations, confirmed by experimental data, revealed that in practice the balls do not separate immediately after leaving the non-synchronous motions area. At first they place themselves in the theoretically unstable position, opposite to the primary unbalance (Figs. 7-9). Only after a certain time, which depends mostly on the level of damping, the balls start moving to the compensation positions. When damping is high as in Fig. 9, the balls may stay in unstable positions for quite a long time.

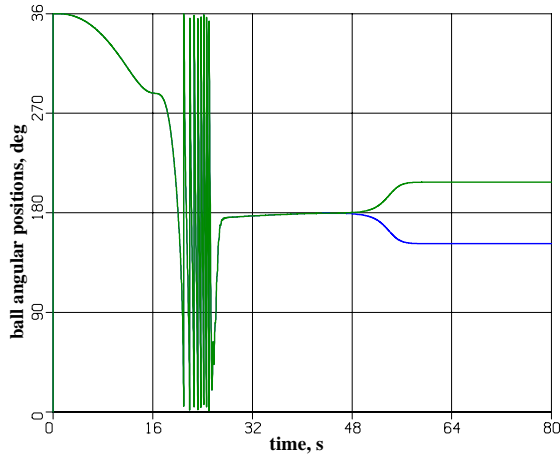


Figure 7. Ball angular positions (wide area of non-synchronous motions).

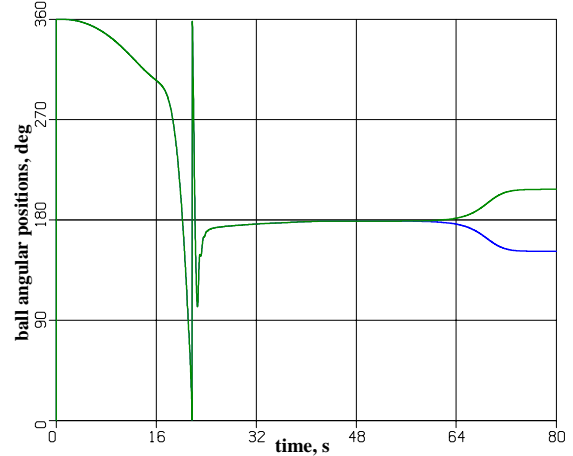


Figure 8. Ball angular positions (medium-wide area of non-synchronous motions).

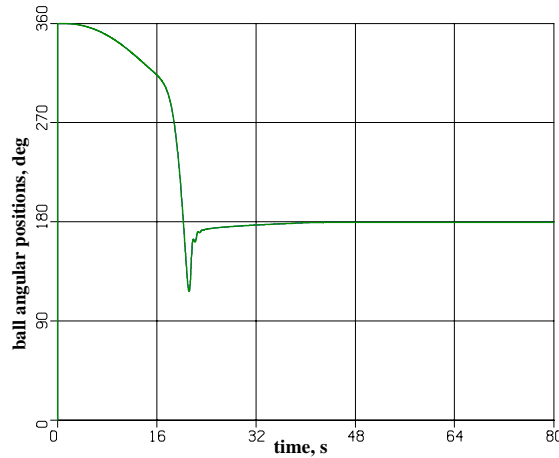


Figure 9. Ball angular positions (narrow area of non-synchronous motions).

4.5 Rotor Vibrations

Figs. 10-12 show rotor vibrations in the plane of the device, when passing the critical speed region. If the area of non-synchronous motions is wide, we observe two maxima of vibrations (Figs. 10,11), which take place, when the rotor and the ball speeds reach resonance points. As demonstrated above, in such cases the balls make several rounds of the track; at certain moments, centrifugal forces from the balls and primary unbalance add to each other, so the maximal vibrations exceed the vibrations engendered by primary unbalance.

When the region of non-synchronous motions becomes narrow, vibrations connected with the primary unbalance and the auto-balancing balls merge with each other more clearly. Here, the initial angular positions of the balls relatively to the primary unbalance play an important role (Fig. 12). For advantageous phasing, the centrifugal forces from the primary unbalance and the auto-balancing balls near the resonance deduct from each other and the vibration level becomes fairly low; for inauspicious phasing these forces add engendering high vibrations.

To provide smooth passing through the critical speed for such type of non-synchronous motions, as in Fig. 12, it is necessary to control the initial phasing. The authors are working in this direction and some first results are presented in the paper (Ryzhik et al., 2003a), submitted to the ASME Conference, but at the moment it is not completely clear whether it is really possible to obtain advantageous phasing in all cases and how complicated the algorithm of control would be.

If the control of initial phasing is not performed, the optimal area of non-synchronous motions looks like in Figs. 8,11. To obtain such area, it is necessary to select carefully the parameters of the device. It is clear that the ball masses and eccentricities should be kept on the lowest possible level, based on the estimation of primary unbalance, because it allows to minimize unbalanced centrifugal forces. The main parameter, which can be used for the “regulation” of non-synchronous motions, as well as for the influence on the process of synchronization with unbalance compensation in the post-critical region, is the damping parameter, β_b . Our investigations have proved that by careful selection of damping it is possible to improve sufficiently the vibration performance of rotor systems with an auto-balancing device in comparison with “not-optimized” cases. More details on the optimization of damping and selection of device parameters can be found in the paper (Ryzhik et al., 2003b).

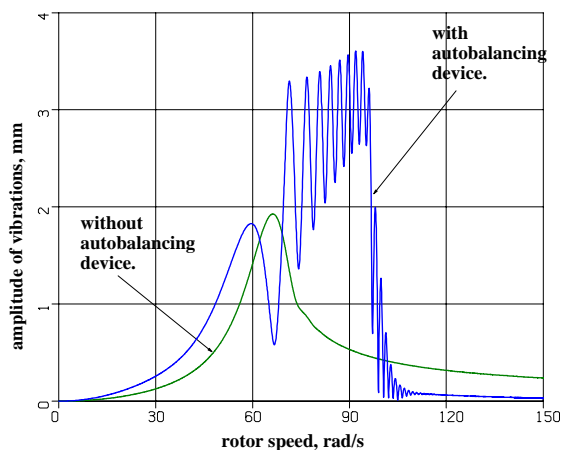


Figure 10. Rotor vibrations in the plane of the device (wide area of non-synchronous motions).

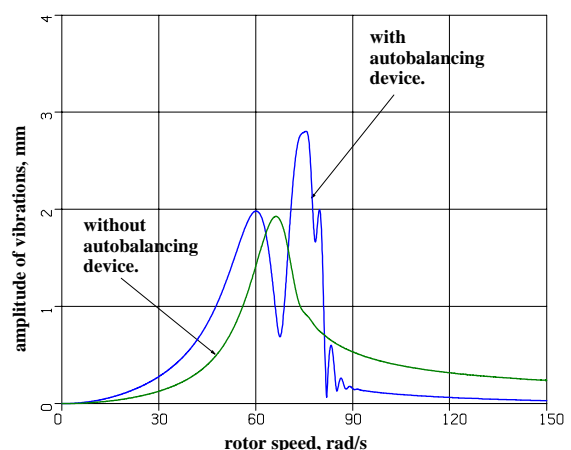


Figure 11. Rotor vibrations in the plane of the device (medium-wide area of non-synchronous motions).

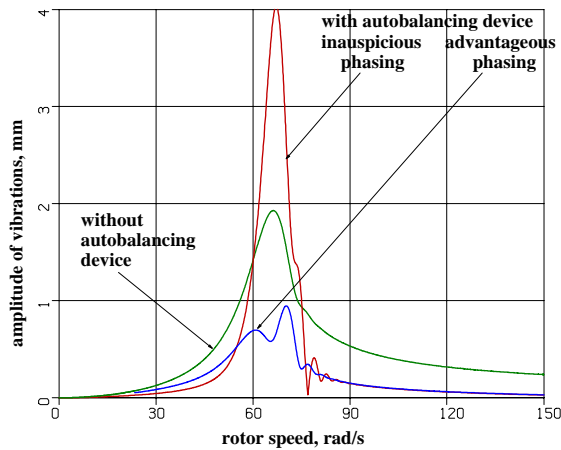


Figure 12. Rotor vibrations in the plane of the device (narrow area of non-synchronous motions).

5 Experimental Verification

The presented results were verified and complemented by experimental data obtained from test runs of the centrifuge rotor system with the auto-balancing device. At the moment, the authors are preparing a paper with a detailed description of these results. It is necessary to emphasize that the agreement between the simulation and experimental data is fairly good.

Many interesting results were also obtained at the experimental set-up in the Otto-von-Guericke-Universität Magdeburg. A description of the set-up equipment and the first results were published in (Gröbel et al., 2003).

6 Conclusion

The presented investigations demonstrate that the non-synchronous motions can sufficiently influence the vibration performance of rotor systems with auto-balancing devices. To provide smooth passing through the critical speed areas, it is necessary to carefully select the device parameters. The authors intend to continue their studies, focusing on the effects of partial unbalance compensation, non-synchronous motions of the balls, as well as on the problems of parameter optimization and phase control.

The most important practical applications of auto-balancing devices are centrifuges, hand power tools, washing machines, and optical disk drives.

Acknowledgements

The authors would like to express their gratitude to the Deutsche Forschungsgemeinschaft for financial support (No. SP 462/7-3).

References

- Blekhman, I.I.: *Vibrational Mechanics*. World Scientific, Singapore, New Jersey, London, Hong Kong, (2000), 509
- Bövik, P.; Högfors, C.: Autobalancing of rotors. *J. of Sound and Vibration*, 111, 3, (1986), 429 – 440
- Chung, J.; Ro, D.S.: Dynamical analysis of an automatic dynamic balancer for rotating mechanisms. *J. of Sound and Vibration*, 228, 5, (1999), 1053 – 1056
- Duckstein, H.; Sperling, L.; Merten, F.: Zum Anlaufproblem beim automatischen Wuchten. *ZAMM* 79, (1999), 2, 285 – 286.
- Gröbel K.-H.; Duckstein H.; Ryzhik B.; Sperling L.: Experimentelle Untersuchungen des selbsttätigen Auswuchtens in zwei Ebenen. In H. Irretier, R. Nordmann & H. Springer (Eds): *Schwingungen in rotierenden Maschinen VI*, Darmstadt, (2003), 133 – 143
- Hedaya, M.T.; Sharp, R.S.: An analysis of a new type of automatic balancer. *J. Mechanical Engineering Science*, 19, 5, (1977), 221 – 226
- Huang, W.-Y.; Chao, C.-P.; Kang, J.-R.; Sung, C.-K.: The application of ball-type balancers for radial vibration reduction of high speed optic drives. *Journal of Sound and Vibration*, 250, 3, (2002), 415 – 430
- Kang, J.-R.; Chao, C.-P.; Huang, C.-L.; Sung, C.-K.: The dynamics of a ball-type balancer system equipped with a pair of free-moving balancing masses. *Transactions of the ASME*, 123, (2001), 456 – 465
- Olsson K.-O.: Limits to the use of auto-balancing. *Proceedings of the 6th Int. Conf. on Rotor Dynamics*. Sydney, 1, (2002) 137 – 145
- Ryzhik, B.; Amer, T.; Duckstein, H.; Sperling, L.: Zum Sommerfeldeffekt beim selbsttätigen Auswuchten in einer Ebene. *Technische Mechanik*, 21, 4, (2001), 297 – 312
- Ryzhik, B.; Duckstein, H.; Sperling, L.: Partial compensation of unbalance by the one- and two-plane automatic balancing devices. *Proceedings of the 6th Int. Conf. on Rotor Dynamics*. Sydney, 1, (2002a), 446 – 455
- Ryzhik, B.; Sperling, L.; Duckstein, H.: The display of Sommerfeld-effect in a rigid rotor one-plane autobalancing device. *Proceedings XXX Summer School "Advanced Problems in Mechanics"*, St. Petersburg, (2002b), 554 – 563
- Ryzhik, B.; Sperling, L.; Duckstein, H.: Problems of Vibrations near Critical Speeds in Rigid Rotors with Autobalancing Devices. *Submitted to the ASME 2003 DETC*, USA, (2003a)
- Ryzhik, B.; Sperling, L.; Duckstein, H.: The Influence of Damping on the Efficiency of Autobalancing Devices for Rigid Rotors. *Proceedings of The Second International Symposium on Stability Control of Rotating Machinery ISCORMA-2003*, Gdańsk Poland, (2003b), 104 – 113
- Sperling, L.; Duckstein, H.: Zum selbsttätigen Auswuchten des starren Rotors in zwei Ebenen. In H. Irretier, R. Nordmann & H. Springer (Eds): *Schwingungen in rotierenden Maschinen V*, Wien, (2001a), 161 – 168
- Sperling, L.; Ryzhik, B. and Duckstein, H.: Two-plane automatic balancing. *Machine Dynamics Problems*, 25, 3/4, (2001b), 139 – 152
- Sperling, L.; Ryzhik, B.; Linz, Ch.; Duckstein, H.: Simulation of two-plane automatic balancing of a rigid rotor. *Mathematics and Computers in Simulation*, 58, (2002), 351 – 365
- Thearle, E.L.: A new type of dynamic-balancing machine. *Transactions of the ASME*, 54, 12 (1932), 131 – 141

Address: Dr.-Ing. Boris Ryzhik, Prof. Dr.-Ing. habil. Lutz Sperling and Dr.-Ing. Henner Duckstein, Institut für Mechanik, Otto-von-GuerickeUniversität Magdeburg, Universitätsplatz 2, 39106 Magdeburg.
email: Boris.Ryzhik@mb.uni-magdeburg.de, Lutz.Sperling@mb.uni-magdeburg.de, Henner.Duckstein@mb.uni-magdeburg.de